Semnan University

Innovations in Materials: Current & Future

Journal homepage: https://imcf.semnan.ac.ir

ISSN: 3115-9990

Research Article

The Effect of Spark Plasma Sintering on Densification, Mechanical Properties, and Crystallographic Texture of $LaMgAl_{11}O_{19}$

Mohammad Mehdi Khorramirad [a]*, Sanaz Hasanzadeh [a], Mohammad Reza Rahimipour [b], Mohammad Mehdi Hadavi [c], Kourosh Shirvani [d]

[a] *Faculty of Materials and Metallurgical Engineering, Semnan University, Semnan, Iran*

[b] *Ceramic Department of Materials and Energy Research Center (MERC), Karaj, Alborz, Iran*

[c] *Department of Materials Engineering, Tarbiat Modares University, Tehran, Iran*

[d] *Department of Advanced Materials and New Energies, Iranian Research Organization for Science and Technology (IROST), Tehran, Iran*

ARTICLE INFO

Article history:

Received: 2025-11-22

Revised: 2025-12-16

Accepted: 2025-12-21

Keywords:

Lanthanum Magnesium Hexaaluminates (LaMgAl11O19);

Spark Plasma Sintering;

Crystallographic Texture;

Densification;

Mechanical Properties;

ABSTRACT

Lanthanum Magnesium Hexaaluminate ($LaMgAl_{11}O_{19}$, LaMA) is a promising material for various applications, including thermal barrier coatings, catalysts, and optical materials, due to its unique properties such as high-temperature thermodynamic and structural stability, low thermal conductivity, and good chemical resistance. In this study, the densification of synthesized LaMA powder was investigated using spark plasma sintering (SPS). The effects of SPS on the relative density, mechanical properties, and crystallographic texture were evaluated. The results showed that SPS achieved a high relative density of 97.56 ± 0.25% and a flexural strength of 367± 13 MPa, which is in good agreement with the findings of other researchers. Remarkably, X-ray diffraction analysis revealed the development of a strong crystallographic texture in the sintered body, characterized by a significant preferential orientation of the (006) plane (Texture Coefficient = 2.82). Scanning electron microscopy confirmed microstructural rearrangement and grain growth. The formation of this textured microstructure, attributed to the preferential alignment of platelet-like grains under uniaxial pressure during SPS, is a key finding of this work and contributes to the understanding of structure-property relationships in SPS-processed hexaaluminates.

1. Introduction

Lanthanum magnesium hexaaluminate is a promising material for thermal barrier coatings (TBCs) due to its exceptionally high-temperature properties. Researchers have explored various synthesis methods, including solid-state reaction [1,2] and sol-gel methods[1,3], to produce LaMA with different compositions and processing parameters. Compared to other magnesium hexaaluminates ($LnMgAl_{11}O_{19}$ with Ln = Nd, Gd), LaMA exhibits superior characteristics for TBC applications[3–6]. Notably, LaMA possesses excellent thermal stability, high resistance to sintering, good fracture toughness, and a long thermal cycling lifetime[7–9]. These advantages are attributed to its unique microstructure, character-

* **Corresponding author.** Tel.: +98 901 691 5570; fax: +98 233 153 3412
E-mail address: *mm.khorramirad@semnan.ac.ir (M. M. Khorramirad)*

Cite this article as:
Khorramirad, M.M., Hasanzadeh, S., Rahimipour, M.R., Hadavi, M.M. and Shirvani, K., 2026. The Effect of Spark Plasma Sintering on Densification, Mechanical Properties, and Crystallographic Texture of LaMgAl11O19. Innovations in Materials: Current & Future, [1(1)], pp. 27-36.
https://doi.org/[Your-Assigned-DOI]

ized by irregular platelet-like grains that contribute to microporosity and low thermal conductivity[7,10]. Beyond TBCs, LaMA finds applications in diverse fields due to its versatility. It serves as a material for lasers and luminescence, catalyst supports, high-temperature catalysts, and nuclear waste immobilization [6,11].

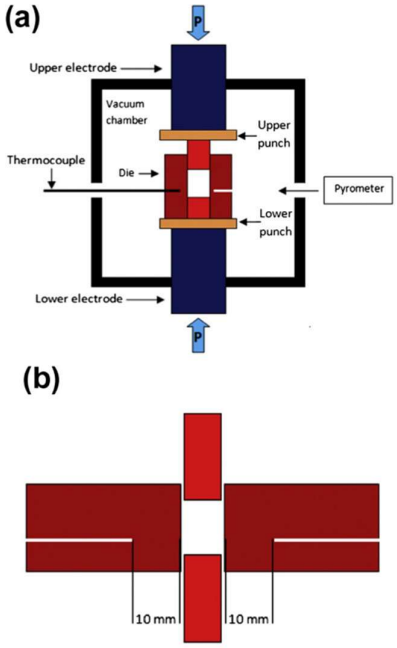

Fig. 1. Schematic of Spark Plasma Sintering (SPS) Equipment [21].

Spark Plasma Sintering (SPS), also known as Field-Assisted Sintering Technique (FAST) or Pulsed Electric Current Sintering (PECS), is a novel powder consolidation technique gaining significant interest due to its several advantages over conventional sintering methods [12–15]. SPS offers lower sintering temperatures, shorter processing times, and improved material properties, making it a versatile tool for a wide range of materials, including conductive and non-conductive powders, ceramics, metals, and composites [16–20]. In the SPS process, a powder compact is placed in a graphite die, and uniaxial pressure is applied while simultaneously passing a pulsed DC through the die and the powder compact [14,16]. The Joule heating generated by the current rapidly raises the temperature of the powder compact, leading to densification and consolidation [19]. The exact mechanisms involved in SPS are still under debate, but Joule heating at particle contacts and enhanced diffusion are believed to play key roles. Some studies suggest that a "spark plasma" may not be present, particularly with non-conductive powders [14,19]. SPS has shown particular promise in the development of new materials and coatings. For instance, researchers have successfully fabricated multi-layered thermal barrier coatings (TBCs) using SPS in a single step [16,18]. The rapid processing and ability to form dense microstructures make SPS a valuable tool for advanced material development [17,18].

In this study, lanthanum hexaaluminate powder synthesized by the solid-state method was used to prepare a high-density sample using the SPS method. However, the specific effects of SPS on the crystallographic texture evolution and its direct link to the mechanical properties of LaMA remain largely unexplored. This study aims to address this gap by systematically investigating the microstructure, crystallographic texture, and mechanical properties of the SPSed sample.

2. Materials and Methods

2.1. Powder Synthesis

The LaMA powder was synthesized using a solid-state reaction method as described in previous studies[6,7]. The details of the synthesis procedure can be found in these references.

2.2. Spark Plasma Sintering (SPS) Densification

Table 1. Parameters of the Spark Plasma Sintering (SPS) process used in this study.

Parameter	Value / Specification
SPS Apparatus	SPS-20T-10
Powder Material	$LaMgAl_{11}O_{19}$
Die Material & Inner Diameter	Graphite, 30 mm
Foil	0.5 mm (Graphite)
Maximum Temperature	1400 °C
Hold Time at Tmax	~5 minutes
Applied Pressure	25 MPa
Heating Rate	~67 °C/min (up to 1000°C) ~29 °C/min (1000°C to 1400°C)
Atmosphere	Vacuum
Temperature Control	Optical pyrometer
Onset of Active Sintering	~1142 °C
Total Punch Displacement	8.3 mm
Total Cycle Time	~33 minutes

The synthesized LaMA powder was densified using spark plasma sintering (SPS). In this

process, a graphite die with an inner diameter of 30 mm is loaded with the powder. A graphite foil is placed between the powder and the die walls to prevent contamination. The SPS apparatus (Fig. 1) applies a high pressure (25 MPa in this case) and pulsed direct current to the die. This combination of pressure and pulsed heating efficiently consolidates the powder particles into a dense LaMA sample. After sintering, the SPS process allows the sample to cool down to room temperature within the chamber. The detailed parameters of the SPS process are summarized in Table 1.

2.3. Mechanical Testing

Three flexural strength specimens with dimensions of 25 × 5 × 3 mm were cut from the sintered sample. Three-point bending tests (Fig. 2) were performed on the specimens using a Santam-STM 20 machine at a crosshead speed of 0.5 mm/min. The flexural strength was calculated using the following equation:

$$\sigma = \frac{3FL}{2bh^2} \quad (1)$$

where: σ is the flexural strength (MPa), F is the load at fracture (N), L is the distance between the supports (mm), b is the width of the specimen (mm), h is the height of the specimen (mm)

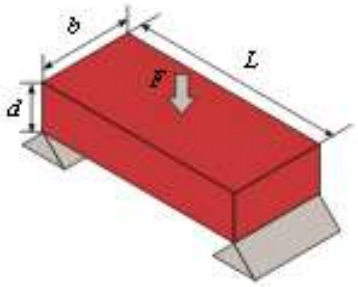

Fig. 2. Schematic of the Three-point Bend Test.

2.4. Phase Analysis

Phase analysis was performed using X-ray diffraction (XRD) with a Siemens D500 diffractometer using Cu(Kα) radiation with a wavelength of 1.5406 Å. The scanning range was from 10° to 80° with a step size of 0.02°.

2.5. Microstructural Analysis

The microstructure of the synthesized powder and sintered samples was examined using a VEGA-TESCAN scanning electron microscope (SEM). The samples were coated with a thin layer of gold before SEM analysis.

2.6. Bulk and Relative Density Measurement

The bulk and relative density of the sintered LaMA sample were measured using Archimedes' method. The weight of each sample was measured in air (dry weight) and then suspended in distilled water (wet weight). The weight of the sample submerged in water (buoyant weight) was also measured. The theoretical density of LaMA used for the calculations was 4.26 g/cm^3. The density was measured for three individual samples. The calculated bulk and relative densities will be presented as average values with standard deviations.

3. Results and Discussions

3.1. Powder Characterization and Phase Analysis

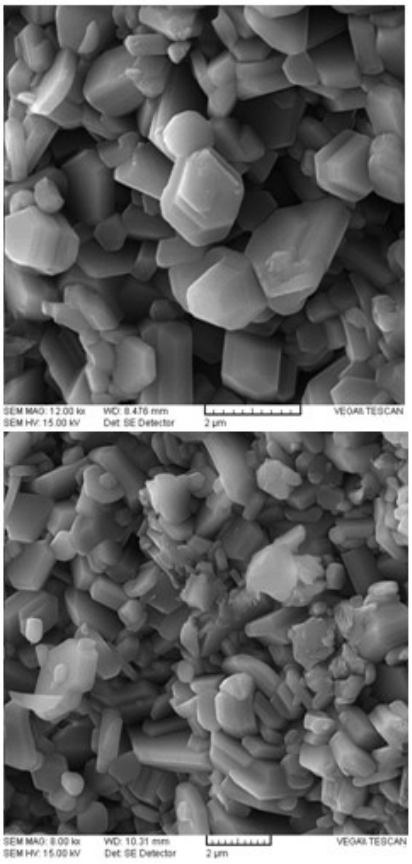

Fig. 3. Scanning Electron Microscopy (SEM) Image of Synthesized LaMA Powder[6,7].

Initial characterization of the starting powder confirmed its suitability for SPS processing. The morphology of the LaMA powder used in this study is characterized by small plates with a high aspect ratio and an approximate thickness of 446 nm, as shown in Fig. 3 [6,7]. This morphology is

consistent with observations in other studies. The observed platelet-like morphology aligns with the crystallographic growth habits of hexaaluminates, where the [0001] crystallographic direction of LaMA has the lowest growth rate, which likely contributes to the development of these platelet-like particles [22,23].

Phase analysis using X-ray diffraction (XRD), as shown in Fig. 4, confirms the formation of the LaMA phase as a single phase. The diffraction pattern of the white synthesized powder matches JCPDS cards numbered 00-026-0873 and 00-078-1845, further supporting the LaMA phase identification [6,7].

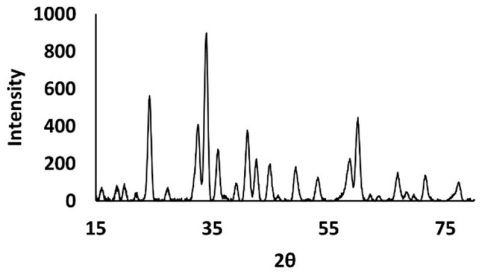

Fig. 4. XRD Pattern of Spark Plasma Sintered (SPS) LaMA Powder[6,7]

3.2. SPS Densification Behavior

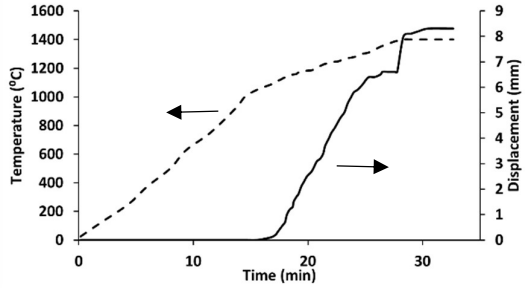

Fig. 5. Displacement, Time, and Temperature (DTT) Diagram for Spark Plasma Sintered (SPS) LaMA Powder.

The densification kinetics during SPS were monitored in real-time, revealing the rapid consolidation characteristics of the process. Fig. 5 shows the effect of punch displacement and temperature changes over time during the SPS process. As sintering time increases, the density of the LaMA sample also increases, reaching a final density. This rapid densification is attributed to the combined effects of Joule heating, which rapidly raises the temperature within the powder compact, and the applied pressure, which promotes particle rearrangement and consolidation. Notably, the average heating rate in SPS is approximately 50-60 °C/min, significantly faster compared to conventional sintering (typically 10 °C/min). This rapid heating facilitates enhanced diffusion mechanisms while suppressing excessive grain growth.

Figs. 6 and 7 further detail the changes in displacement (indicating shrinkage) as a function of temperature and time during SPS, respectively. The analysis of these figures reveals that the densification process, characterized by a positive shrinkage rate, commences at approximately 1000 °C and concludes at 1400 °C, where the shrinkage rate returns to zero. The total amount of shrinkage observed was 6.6 mm before the final pressure increase and reached 8.1 mm after applying the pressure (Fig. 7).

3.3. Microstructural Evolution

SPS processing induced significant microstructural reorganization, as evidenced by detailed microscopic examination. Fig. 8 shows the surface morphology of the Spark Plasma Sintered (SPS) sample. As can be observed, the LaMA plate-shaped particles are arranged in groups, oriented along the thickness and at an angle to the sample surface, exhibiting a specific type of organization. This oriented structure might influence the mechanical properties of the LaMA sample. These observations are further supported by the changes in the X-ray diffraction (XRD) patterns of the powder particles and the SPS sample, presented in Figs. 4 and 9. The most significant changes in the XRD patterns are observed in the (107), (114), (006), and (205) planes, with the most prominent differences appearing in the (006) and (107) planes. The preferential orientation of the platelet-like particles during SPS may contribute to the observed variations in the XRD patterns.

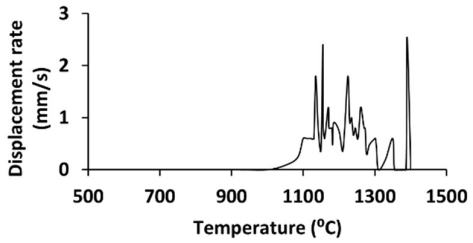

Fig. 6. Displacement Rate vs. Sintering Temperature Diagram for Spark Plasma Sintered (SPS) LaMA Powder.

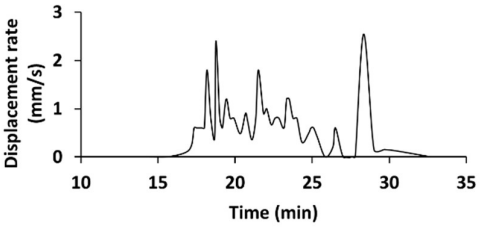

Fig. 7. Displacement Rate vs. Sintering Time Diagram for Spark Plasma Sintered (SPS) LaMA Powder.

3.4. Mechanical Properties

The microstructural development during SPS directly translated to enhanced mechanical performance. Load-displacement curves obtained from three-point bend tests are used to determine various mechanical properties of materials, including flexural strength, Young's modulus, and fracture toughness.

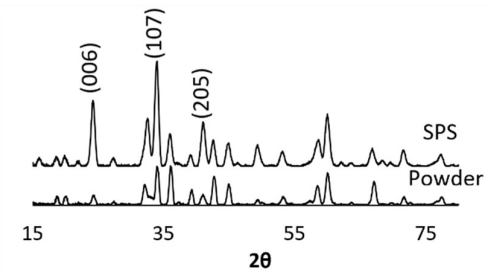

Fig. 9. Comparison of XRD patterns of powder synthesized at 1600 °C and the SPS sample.

Fig. 10 illustrates the load-displacement curves for three lanthanum hexaaluminate ceramic samples. The curves show the relationship between the applied load and the displacement of the center of the sample. All three curves exhibit similar overall shapes, suggesting a comparable mechanical response of the samples. However, slight variations in the maximum load and fracture point between the curves indicate some microstructural or property variations among the samples. The samples exhibit brittle behavior, characterized by a sharp drop in load after the fracture point. Using Eq. (1) and considering the gauge length, the flexural strength of the samples was calculated. The average flexural strength obtained from three tests for the lanthanum hexaaluminate ceramics was 367 ± 13 MPa.

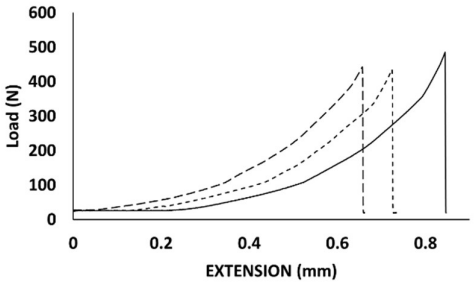

Fig. 10. The load-displacement curve of the three-point bend test for three lanthanum hexaaluminate ceramic samples.

The achieved mechanical properties demonstrate significant improvement over conventional processing routes. Jiang et al. achieved a relative density of 95.9% using cold isostatic pressing (CIP) at 250 MPa and sintering at 1700 °C for 6 hours [24]. In contrast, this study employed Spark Plasma Sintering (SPS) to achieve a higher relative density of 97.56% with significantly lower pressure (25 MPa), temperature (1400 °C), and shorter processing time (35 minutes) compared to CIP, as shown in Table 2.

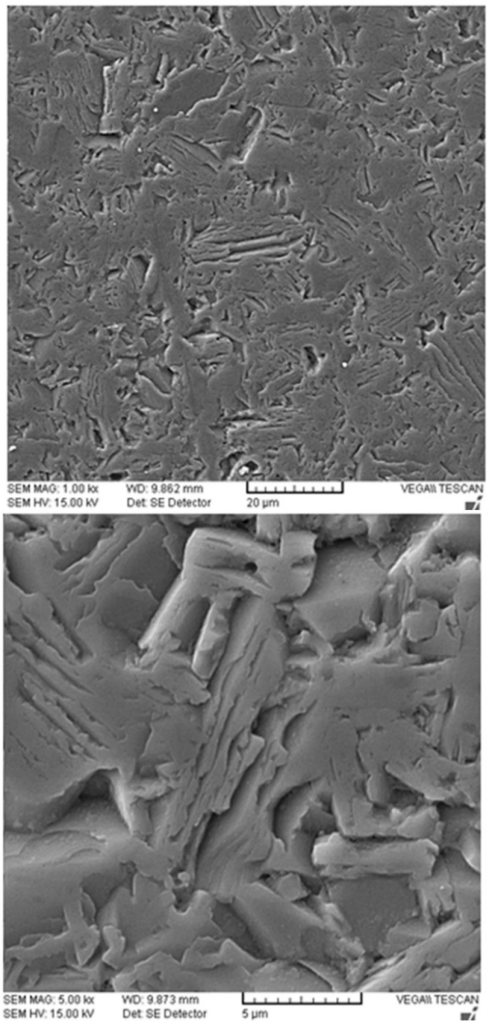

Fig. 8. SEM image of the surface morphology of an SPS sample.

Table 2. Properties of Spark Plasma Sintered (SPS) LaMA Composition

Sample	LaMA
Relative Density (%)	97.56 ± 0.25
Theoretical Density(g/cm^3)	4.26
Water Absorption (%)	0.031 ± 0.005
Porosity (%)	2.44 ± 0.23
Archimedes' Density(g/cm^3)	4.156 ± 0.011
Buoyant Weight (g)	6.8487
Wet Weight (g)	9.0179
Dry Weight (g)	9.0151

3.5. Crystallographic Texture Analysis

Crystallographic texture analysis through X-ray diffraction provides critical insights into orientation development in LaMA hexaaluminate during processing. The texture coefficient (TC), calculated according to Eq. 2, serves as a fundamental quantitative parameter for characterizing crystallographic orientation in polycrystalline materials[25,26].

$$TC(hkl) = \frac{\frac{I(hkl)}{I_0(hkl)}}{\frac{1}{N}\sum\frac{I(hkl)}{I_0(hkl)}} \quad (2)$$

Where I(hkl) is the measured intensity, I0(hkl) is the reference intensity, and N is the number of diffraction peaks [25,26]. This parameter provides critical insights into material anisotropy, with TC > 1 indicating preferred orientation, TC < 1 showing suppressed growth, and TC = 1 representing random crystallite distribution. The analysis proves particularly valuable for understanding anisotropic growth phenomena in complex crystal systems, enabling precise correlation between processing conditions and resulting microstructural characteristics. For hexaaluminate compounds like LaMA, TC quantification reveals essential platelet growth mechanisms and orientation development during synthesis, offering a powerful tool for optimizing material performance in applications where crystallographic texture governs functional properties. The method's quantitative nature enables systematic comparison of texture evolution under varying processing parameters, thereby establishing reliable structure-property relationships in advanced crystalline materials.

The initial powder synthesized by the solid-state method exhibits nearly random crystallographic orientation, as evidenced by TC values approximating unity across most crystallographic planes (Table 3, Fig. 11).

In contrast, Spark Plasma Sintering induces a dramatic microstructural transformation, developing a strong preferential orientation characterized by an exceptionally high TC value for the (006) plane (TC = 2.82) alongside significant suppression of other orientations such as (114) and (220) (TC < 0.3) (Table 4, Fig. 12).

The XRD pattern of the SPS-processed sample (Fig. 9) clearly deviates from random orientation, showing pronounced enhancement of the (107) peak intensity and, to a lesser extent, the (006) and (205) reflections. Structural interpretation reveals that the observed maximum intensity for the (107) plane definitively indicates this plane's preferential alignment parallel to the sample surface, resulting in a "Tilted Basal Texture" where basal (0001) planes tilt approximately 34° relative to the surface (Fig. 13c). This texturing phenomenon is a direct consequence of the unique Spark Plasma Sintering (SPS) conditions, where the applied uniaxial pressure promotes preferential rotation and alignment of platelet-shaped LaMA grains.

Table3. Texture coefficients (TC) of LaMA powder synthesized by the solid-state method.

Texture coefficient (TC)	
Crystallographic Plane (hkl)	Solid-state
(101)	0.764
(102)	1.078
(110)	0.967
(107)	0.964
(114)	0.901
(203)	0.794
(205)	1.005
(206)	1.096
(217)	1.023
(2011)	1.35
(220)	1.062

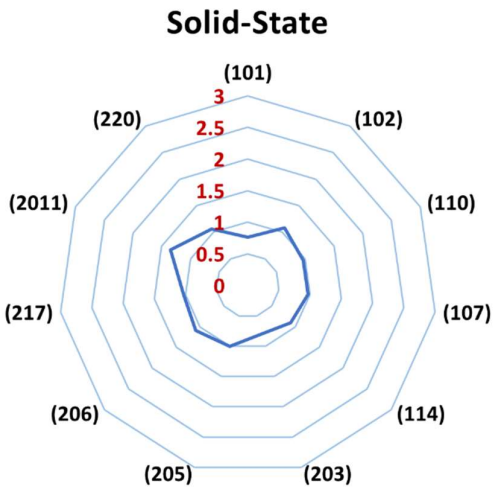

Fig. 11. Radar chart of texture coefficients (TC) for LaMgAl$_{11}$O$_{19}$ powder synthesized by the solid-state method.

The resulting distinct crystallographic alignment is quantitatively substantiated by the angular relationships in Table 5, which reveals a clear correlation: planes with smaller angles to the (0001) basal plane (e.g., (107) with θ = 33.793°) maintain higher TC values, while those perpendicular to it (e.g., (110) with θ = 90°) exhibit

strongly suppressed growth. This mechanism demonstrates excellent consistency with microstructural observations (Fig. 8), the XRD pattern (Fig. 9), and the proposed grain arrangement schematic (Fig. 13). Furthermore, the significant intensity enhancement of the (205) peak indicates the development of a secondary texture component alongside the primary (107) orientation. Collectively, this comprehensive texture analysis establishes robust structure-property relationships that are indispensable for optimizing material performance in applications governed by crystallographic anisotropy.

Table 4. Texture coefficients (TC) of the LaMA SPSed sample.

Texture coefficient (TC)	
Crystallographic Plane (hkl)	SPS
(006)	2.822108
(110)	0.756649
(107)	0.96535
(114)	0.266949
(2011)	0.894668
(220)	0.294275

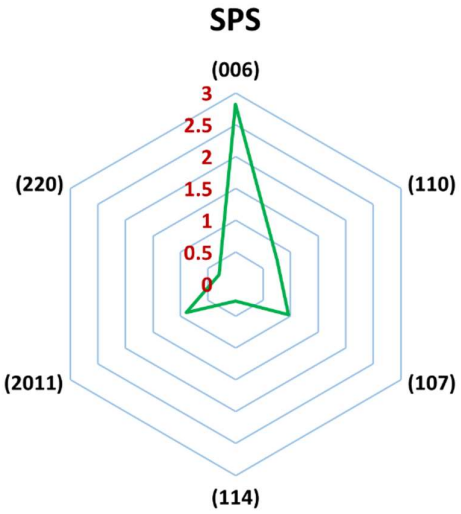

Fig. 12. Radar chart of texture coefficients (TC) for the LaMA pellet densified by Spark Plasma Sintering (SPS).

This study successfully demonstrated the efficacy of Spark Plasma Sintering (SPS) in densifying lanthanum magnesium hexaaluminate and tailoring its microstructure. The SPS process achieved a high relative density of 97.56 ± 0.25 % and a remarkable flexural strength of 367±13 MPa under significantly lower temperature, pressure, and shorter time compared to conventional methods. Most notably, a strong crystallographic texture was quantitatively characterized for the first time in SPSed LaMA, with the (006) plane exhibiting a predominant orientation (Texture Coefficient = 2.82). This texturing, induced by the uniaxial pressure and rapid heating of SPS, resulted in the preferential alignment of the platelet-like grains, as confirmed by both XRD and SEM analyses. The formation of this textured microstructure is a key factor contributing to the enhanced mechanical properties, establishing a direct structure-property relationship. These findings underscore the potential of SPS not only as a densification tool but also as a means to microstructurally engineer hexaaluminate ceramics for superior performance. For future work, it is recommended to investigate the anisotropies of thermal and mechanical properties induced by this texture, as well as the thermal cycling performance of the textured LaMA, to assess its potential for next-generation thermal barrier coating applications fully.

Table 5. Crystallographic orientation analysis showing angular relationships and thickness contributions of different planes relative to the (0001) basal plane.

Crystallographic Plane (hkl)	Angle with (0001) θ (°)	cos(θ)	Thickness Contribution (%)
(101)	77.951	0.209	20.875
(102)	66.882	0.393	39.263
(006)	0	1	100
(110)	90	0	0
(107)	33.793	0.831	83.106
(114)	63.759	0.442	44.215
(203)	72.246	0.305	30.494
(205)	61.914	0.471	47.080
(206)	57.366	0.539	53.928
(217)	60.544	0.492	49.175
(2011)	40.424	0.761	76.127
(220)	90	0	0

1. Conclusions

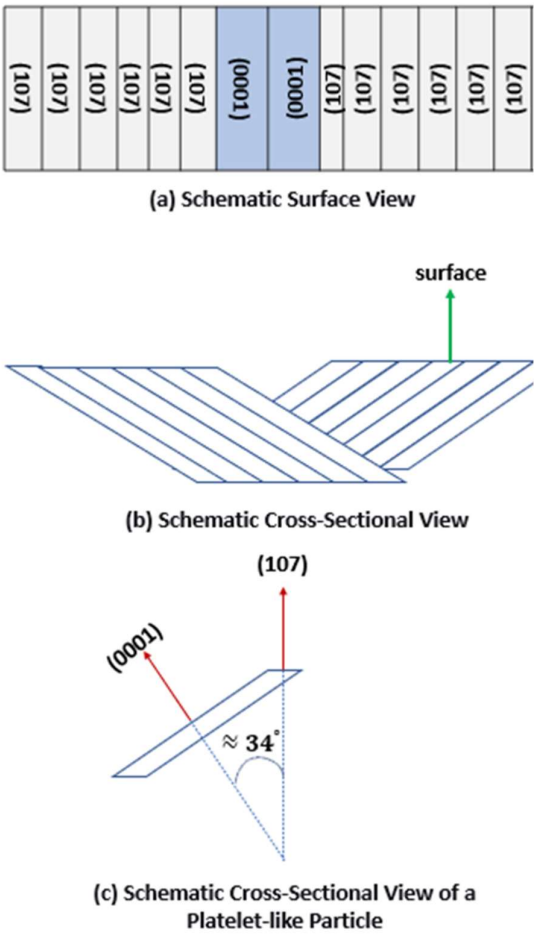

Fig. 13. Schematic diagrams of the developed texture. (a) Surface view of aligned platelets. (b) Cross-section showing the tilt of the grains relative to the pressing surface. (c) Orientation of a single grain, illustrating how the (107) plane being parallel to the surface results in a ~34° tilt of the basal (0001) plane.

Nomenclature

Symbol	Definition (Unit)
B	Width of the specimen (mm)
F	Load at fracture (N)
H	Height of the specimen (mm)
I	Measured diffraction intensity (a.u.)
I_0	Reference diffraction intensity (a.u.)
L	Distance between supports (mm)
N	Number of diffraction peaks
TC	Texture coefficient
Σ	Flexural strength (MPa)
(hkl)	Miller indices

Acknowledgments

Authors employed AI-powered language models to improve language fluency, readability, and proofreading. It is important to note that these tools were used solely for linguistic enhancement, and all scientific content, data interpretation, and conclusions remain the sole responsibility of the authors. After using these tools, the authors reviewed and edited the content as needed and take full responsibility for the content of the publication.

Funding Statement

This research did not receive any specific grant from funding agencies in the public, commercial, or not-for-profit sectors.

Conflicts of Interest

On behalf of all authors, the corresponding author states that there is no conflict of interest.

Authors Contribution Statement

Mohammad Mehdi Khorramirad:
Conceptualization, Methodology, Investigation, Formal Analysis, Writing - Original Draft, Visualization, Supervision, Validation, Writing - Review & Editing, Final Review, Project Administration
Sanaz Hasanzadeh:
Conceptualization, Methodology, Investigation, Experimental Work, Writing - Original Draft, Visualization.
Mohammad Reza Rahimipour:
Supervision.
Mohammad Mehdi Hadavi:
Supervision.
Kourosh Shirvani:
Supervision.

References

[1] D. Stöver, G. Pracht, H. Lehmann, M. Dietrich, J.E. Döring, R. Vaßen, New material concepts for the next generation of plasma-sprayed thermal barrier coatings, Journal of Thermal Spray Technology 13 (2004) 76–83.

[2] X. Chen, Y. Zhao, L. Gu, B. Zou, Y. Wang, X. Cao, Hot corrosion behaviour of plasma sprayed YSZ/LaMgAl11O19composite coatings in molten sulfate-vanadate salt, Corros Sci 53 (2011) 2335–2343.

[3] J. Zhang, X. Zhong, Y. Cheng, Y. Wang, Z. Xu, X. Chen, H. Ma, Y. Zhao, X. Cao, Thermal-shock resistance of LnMgAl11O19(Ln = La, Nd, Sm,

Gd) with magnetoplumbite structure, J Alloys Compd 482 (2009) 376–381.

[4] M.M. Khorramirad, M.R. Rahimipour, S.M.M. Hadavi, K. Shirvani, High temperature oxidation behavior of Inc-738/NiCrAlY/LaMA thermal barrier coating system, Surf Coat Technol 364 (2019) 70–80.

[5] M.M. Khorramirad, M.R. Rahimipour, S.M.M. Hadavi, K. Shirvani, Preoxidation of bond coat in IN-738LC/NiCrAlY/LaMgAl11O19 thermal barrier coating system, Ceram Int 44 (2018) 22080–22091.

[6] M.M. Khorramirad, M.R. Rahimipour, S.M.M. Hadavi, K. Shirvani Jozdani, Synthesis of the lanthanum magnesium hexaaluminate (LaMgAl11O19) powder in order to plasma spray coating on the nickel super alloy as a thermal barrier coating, New Process in Material Engineering 12 (2018) 173–183.

[7] M.M. Khorramirad, M.R. Rahimipour, S.M.M. Hadavi, K.S. Jozdani, The effect of magnesium compounds (MgO and MgAl2O4) on the synthesis of Lanthanum magnesium hexaaluminate (LaMgAl11O19) by solid-state reaction method, Ceram Int 44 (2018) 4734–4739.

[8] X. Chen, B. Zou, Y. Wang, H. Ma, X. Cao, Microstructure and thermal cycling behavior of air plasma-sprayed YSZ/LaMgAl11O19 composite coatings, Journal of Thermal Spray Technology 20 (2011) 1328–1338.

[9] X. Chen, L. Gu, B. Zou, Y. Wang, X. Cao, New functionally graded thermal barrier coating system based on LaMgAl11O19/YSZ prepared by air plasma spraying, Surf Coat Technol 206 (2012) 2265–2274.

[10] S.M. Naga, Ceramic matrix composite thermal barrier coatings for turbine parts, Woodhead Publishing Limited, 2014.

[11] X. Chen, Y. Zhao, W. Huang, H. Ma, B. Zou, Y. Wang, X. Cao, Thermal aging behavior of plasma sprayed LaMgAl11O19thermal barrier coating, J Eur Ceram Soc 31 (2011) 2285–2294. .

[12] J.J.M. Juárez, D. V. Jaramillo, R.A. Cuenca, F.L. Juárez, Sintering comparison of NiCoCrAl-Ta powder processed by hot pressing and spark plasma, Powder Technol 221 (2012) 264–270.

[13] S. Yeo, E. McKenna, R. Baney, G. Subhash, J. Tulenko, Enhanced thermal conductivity of uranium dioxide-silicon carbide composite fuel pellets prepared by Spark Plasma Sintering (SPS), Journal of Nuclear Materials 433 (2013) 66–73.

[14] L. Ge, G. Subhash, R.H. Baney, J.S. Tulenko, E. McKenna, Densification of uranium dioxide fuel pellets prepared by spark plasma sintering (SPS), Journal of Nuclear Materials 435 (2013) 1–9.

[15] Y. Li, K. Hu, X. Li, X. Ai, S. Qu, Fine-grained 93W-5.6Ni-1.4Fe heavy alloys with enhanced performance prepared by spark plasma sintering, Materials Science and Engineering: A 573 (2013) 245–252.

[16] N. Ratel, D. Monceau, C. Estournès, D. Oquab, Reactivity and microstructure evolution of a CoNiCrAlY/Talc cermet prepared by Spark Plasma Sintering, Surf Coat Technol 205 (2010) 1183–1188.

[17] D. Monceau, D. Oquab, C. Estournès, M. Boidot, S. Selezneff, N. Ratel-Ramond, Thermal barrier systems and multi-layered coatings fabricated by spark plasma sintering for the protection of Ni-base superalloys, Materials Science Forum (2010) 1826–1831.

[18] M. Boidot, S. Selezneff, D. Monceau, D. Oquab, C. Estournès, Proto-TGO formation in TBC systems fabricated by spark plasma sintering, Surf Coat Technol 205 (2010) 1245–1249.

[19] R. Ohser-Wiedemann, U. Martin, H.J. Seifert, A. Müller, Densification behaviour of pure molybdenum powder by spark plasma sintering, Int J Refract Metals Hard Mater 28 (2010) 550–557.

[20] Z. Guo, G. Blugan, R. Kirchner, M. Reece, T. Graule, J. Kuebler, Microstructure and electrical properties of Si3N4-TiN composites sintered by hot pressing and spark plasma sintering, Ceram Int 33 (2007) 1223–1229.

[21] M. Kermani, M. Razavi, M.R. Rahimipour, M. Zakeri, The effect of mechanical alloying on microstructure and mechanical properties of MoSi2prepared by spark plasma sintering, J Alloys Compd 593 (2014) 242–249.

[22] X. Chen, Y. Zhao, X. Fan, Y. Liu, B. Zou, Y. Wang, H. Ma, X. Cao, Thermal cycling failure of new LaMgAl11O19/YSZ double ceramic top coat thermal barrier coating systems, Surf Coat Technol 205 (2011) 3293–3300.

[23] X. Chen, Y. Zhang, X. Zhong, Z. Xu, J. Zhang, Y. Cheng, Y. Zhao, Y. Liu, X. Fan, Y. Wang, H. Ma, X. Cao, Thermal cycling behaviors of the plasma sprayed thermal barrier coatings of hexaluminates with magnetoplumbite structure, J Eur Ceram Soc 30 (2010) 1649–1657.

[24] B. Jiang, M.H. Fang, Z.H. Huang, Y.G. Liu, P. Peng, J. Zhang, Mechanical and thermal properties of LaMgAl11O19, Mater Res Bull 45 (2010) 1506–1508.

[25] R. Stylianou, M. Tkadletz, N. Schalk, M. Penoy, C. Czettl, C. Mitterer, Effects of reference materials on texture coefficients determined for a CVD α-Al2O3 coating, Surf Coat Technol 359 (2019) 314–322.

[26] Y. Wang, W. Tang, L. Zhang, Crystalline Size Effects on Texture Coefficient, Electrical and Optical Properties of Sputter-deposited Ga-doped ZnO Thin Films, J Mater Sci Technol 31 (2015) 175–181.